

# Spin-orbit and exchange interaction in surface quantum wells on gapless semimagnetic semiconductor HgMnTe

V.F. Radantsev \*

*Institute of Physics and Applied Mathematics,  
Ural State University, Ekaterinburg 620083, Russia*

A.M. Yafyasov, V.B. Bogevolnov and I.M. Ivankiv

*Department of Solid State Electronics, Institute of Physics,  
St. Petersburg State University, St. Petersburg 198904, Russia*

November 13, 2018

## Abstract

The first study of two-dimensional electron gas in surface layers on HgMnTe with inverted bands is carried out experimentally and theoretically. It is shown that the structure of investigated capacitance magnetooscillations in HgMnTe MOS structures is fully similar to the one in the non-magnetic narrow-gap semiconductor HgCdTe and the sole effect due to exchange interaction is the temperature shift of beat nodes. The information about exchange effects is obtained only due to our modeling of oscillations, because any pronounced changes in the position of oscillations are not observed and the separate spin components are not resolved. The Landau levels are calculated in the framework of concept we developed previously for the description of subband dispersions in zero magnetic field  $B = 0$ . The new parameters (like those of  $T/\sqrt{eB}$ ) arise in the theory of magnetooscillations in the semiconductors with quasirelativistic spectrum in contrast to the case of parabolic bands. The modeling shows that the spin-orbit splitting far exceeds a contribution due to exchange interaction. The calculated amplitudes of “partial” oscillations for different spin branches of spectrum are essentially different in accordance with the observed difference in the intensity of corresponding lines in Fourier spectra. The comparison between experiment and theory for different temperatures and parameters of exchange interaction is reported. The dominant mechanisms of the scattering responsible for the broadening of Landau levels are discussed.

**PACS numbers:** 73.20.Dx, 73.40.Qv, 71.70.Ej

---

\*e-mail: victor.radantsev@usu.ru

# 1 Introduction

There are two aspects that cause the peculiar features of, and the interest in, the two-dimensional (2D) electron gas in narrow-gap diluted magnetic (semimagnetic) semiconductors (DMS). One stems from the  $s, p - d$  exchange interaction between band electrons and localized magnetic moments [1]. This interaction results in changed spin splitting of the band states, which can be varied by such external factors as a magnetic field and temperature. The other is due to the peculiarities inherent to Kane semiconductors with small gap, leading to such relativisticlike effects as non-parabolicity, kinetic confinement (motional binding [2]), spin-orbit (SO) splitting and resonant interband mixing by surface electric field [3, 4, 5]. What is important in the context of the specificity of 2D electronic systems involving DMS, is that both exchange and SO interaction cause the rearrangement of the spin structure of Landau levels (LL's). Although historically the first studies of 2D electron gas in DMS were performed for metal-insulator-semiconductor (MIS) structures based on HgMnTe, [6] the available experimental results are mostly for the grain boundaries in HgMnTe and HgCdMnTe with positive Kane gap  $E_g > 100$  meV at Mn content typically  $x = 0.02$  (for the higher  $x$ , the exchange interaction exhibited itself poorly, that was attributed to antiferromagnetic interaction between Mn ions) [1, 7, 8, 9]. This is due to low electron mobility in previously investigated MIS structures. At the same time, the inversion layers in MIS structures are of particular experimental interest because of the possibility of controlling the depth of surface quantum well by gate voltage, and because of the relative ease and accuracy of the description of surface potential (in the case of the bicrystals, the additional poorly verified assumptions have to be used to describe a self-consistent potential near grain boundaries [10]). An important point is that these results can be compared with the data for MIS structures based on narrow-gap HgCdTe [4, 11], being non-magnetic analogue of narrow-gap DMS.

As regards their theoretical description, the subband calculations were carried out only for DMS with direct but not inverted bands and without allowance for spinorlike effects [1, 6]. However, the SO splitting in asymmetrical quantum wells at zero magnetic field (this phenomenon in itself is of much current interest [4, 5, 12, 13, 14, 15, 16, 17, 18, 19]) leads to the rearrangement of subband magnetic levels. In narrow-gap semiconductors, the perturbation of magnetic spectrum is so drastic that SO interaction cannot be neglected in the theoretical treatment. It must be stressed that SO splitting, as we shall see in Sec. III, exceeds by far exchange interaction contribution so it cannot be considered as a correction to the exchange interaction. It is clear also that a treatment based on the quasiclassical quantization in a magnetic field of subband spectrum (calculated at  $B = 0$ ) is unsuitable for the description of exchange interaction effects. A more rigorous theoretical consideration of the LL's structure is required.

In this paper, the peculiarities of 2D electron gas due to exchange and SO interaction are studied in inversion layers on  $\text{Hg}_{1-x}\text{Mn}_x\text{Te}$ . with a small Mn content. At  $x < 0.08$  HgMnTe has inverted bands (i.e. becomes semimetal) and traditional galvanometric methods cannot be used because of the shunting of surface conductance by the bulk. We employed the magnetocapacitance spectroscopy method, which is applicable to semiconductors with any sign of the Kane gap. The parameters of the samples and the experimental data relating to the capacitance oscillations versus gate voltage and magnetic field and their tempera-

ture evolution are presented in Sec. II. In Sec. III, we present the theoretical model. The treatment of LL's in 2D subbands is based on the further development of the concept we offered previously for the description of subband spectrum at  $B = 0$ . The density of states (DOS) in a magnetic field is described neglecting the mixing between LL's and assuming a Gaussian shape of each level. In this section an analytical expression for oscillations of the differential capacitance of space charge region in the low-temperature range is also obtained using WKB approach. In Sec. IV, the results of the computer modeling of capacitance oscillations are presented. The results of a comparison of the experimental data and theoretical calculations for different temperatures and parameters of exchange interaction are discussed. The parameters of the broadening of LL's are determined from a fitting of the amplitudes of calculated oscillations to their experimental values. The dominant mechanisms of the scattering responsible for broadening of LL's are discussed.

## 2 Samples and experimental results

### 2.1 Samples and experimental methods

In this work the inversion layers in MIS structures fabricated from  $p$ -Hg<sub>1-x</sub>Mn<sub>x</sub>Te single crystals were investigated. No impurities were introduced intentionally and no post growth annealing was performed. Deviations from stoichiometry, and thus the type of the conductivity, were controlled by mercury partial pressure during the growth process. The Hall-effect measurements were performed at variable temperatures and magnetic field strengths. After removing the Hall and tunnel contacts (see below), the substrates were mechanically polished and etched in a 0.5 bromine-methanol solution. Several methods such as anodic oxide formation, silicon oxide and Al<sub>2</sub>O<sub>3</sub> deposition, and the Langmuir-Blodgett film technique have been used for forming an insulating film in MIS structures. The gate electrodes of the typical area  $\sim 5 \times 10^{-4}$  cm<sup>2</sup> were formed evaporating Pb. The differential capacitance  $C$  and derivative  $dC/dV_g$  on gate voltage  $V_g$  of the capacitors were measured in the dark, typically at 1 MHz and a test signal amplitude of 5 mV.

The capacitance magnetooscillations due to the magnetic quantization of 2D electron gas were observed in all the above HgMnTe MIS structures. It was shown that the general shapes of the oscillations at the same carrier surface density and Mn content are similar. In the following we present the results for the structures with a  $\sim 80$  nm thick anodic oxide film, grown in a solution of 0.1M KOH in 90% ethylene glycol / 10% H<sub>2</sub>O at 0.1 mA·cm<sup>-2</sup>. There are several reasons for such a choice: (i) the amplitudes of oscillations in these structures are the highest owing to the large value of insulator capacitance (this is caused by the large value of dielectric constant of the anodic oxide), (ii) the highest surface carrier densities are achieved at low gate voltages  $V_g = 10 - 15$  V, and (iii) the dielectric constant of oxide is close to that of a semiconductor so the contribution of image forces in surface potential can be neglected in the calculations.

We investigated samples with different Mn content ( $x = 0.024, 0.040, 0.060$  and  $0.1$ ). Kane gap  $E_g$  and Kane effective mass  $m_b$  (and therefore  $x$ ) were determined independently by the tunnel spectroscopy method for a comparison of band parameters in the bulk with those in the vicinity of the surface. The discrepancy is within the accuracy of the analysis ( $\Delta x \sim 0.002 \div 0.003$ ). Because the tunnel contacts and studied MIS capacitors were

produced using identical technology and differ only by thickness of insulator (Langmuir-Blodgett film or an oxide) this agreement testifies that the surface layers are chemically close to the bulk. The similarity of the results for the structures with different insulators (with different fabrication methods) supports this conclusion. The fact that in the small surface concentration range the measured cyclotron masses in 2D subbands extrapolate to the bulk value  $m_b$  is direct evidence of an absence of noticeable decomposition in 2D layer during the structure fabrication process.

In the following we shall restrict our consideration to the results for HgMnTe with  $x \approx 0.04$  ( $E_g = -100 \pm 5$  meV). The amplitudes of the oscillations for other samples are much less even at 4.2 K and rapidly decrease with increasing temperature. In the case of  $x \approx 0.024$  this is caused by the small cyclotron energy due to a large Kane gap. In the cases  $x \approx 0.06$  and  $x \approx 0.1$  it is due to the large doping level of available materials. As a result, we could not obtain reasonably accurate information about the oscillation's temperature evolution, in which the specificity of DMS is manifested. As to the measurements at  $T = 4.2$  K, the subband parameters extracted from oscillations for these samples are similar to those for HgCdTe with the same band parameters and agree well with the theory. On the other hand, the samples with  $x = 0.04$  are best suited to the purpose of this first study aimed at investigating the peculiarities of 2D electron gas in DMS with inverted bands, in which (i) the effects of SO and exchange interaction are expected to be more clearly pronounced and (ii) the results can be compared with those for well studied surface layers on gapless HgCdTe with  $E_g \sim -(50 \div 100)$  meV [4, 20]. For small gap  $|E_g| < 100$  meV the parameters of 2D subbands depend only weakly on  $E_g$  (except in the case of small subband occupancies). [4, 20] By contrast, the subband parameters are more sensitive to the doping level. For this reason, we present the results for two samples with  $N_A - N_D = 1.2 \times 10^{16} \text{ cm}^{-3}$  (sample *S1*) and  $N_A - N_D = 1.5 \times 10^{17} \text{ cm}^{-3}$  (sample *S2*). The Hall mobility of holes is of the order of  $2500 \text{ cm}^2/\text{Vs}$  at 4.2 K. The experimental data are presented below for capacitors with the gate area  $S = 7.2 \times 10^{-4} \text{ cm}^2$  and insulator capacitance  $C_{ox} = 136.5 \text{ pF}$  for sample *S1*, and with  $S = 7.7 \times 10^{-4}$  and  $C_{ox} = 155.1 \text{ pF}$  for sample *S2*.

## 2.2 Capacitance measurements in perpendicular magnetic fields

Fig. 1 shows the capacitance-voltage characteristics at  $T = 4.2$  K in magnetic field  $B = 4.5$  T perpendicular to the 2D layer for the sample *S2*.  $C(V_g)$  characteristics are those of typical low-frequency behavior. This is due to the absence of a gap between conduction and valence (heavy hole) band in gapless semiconductors. As a result, 2D electrons in inversion layers are in equilibrium with the ac ripple and contribute predominantly to the measured capacitance under inversion band bending. The low-frequency conditions with respect to the minority carriers are satisfied in all the investigated frequency range  $30 \text{ kHz} \div 5 \text{ MHz}$ . The wide hysteresis loop and the dependence of  $C(V_g)$  characteristics on the rate of voltage sweep are observed. The capacitance changes in time because of flat-band voltage shift  $\Delta V_{fb}$ , which is close to logarithmic in time. The time constant is of the order of a few minutes and is almost independent of the temperature. The hysteresis effects point to charge tunnel exchange between the semiconductor and the slow traps in insulator [21]. A history dependence and instability are manifested in all the investigated HgMnTe-based MIS structures. Such behavior is contrary to that of HgCdTe and HgTe-based structures

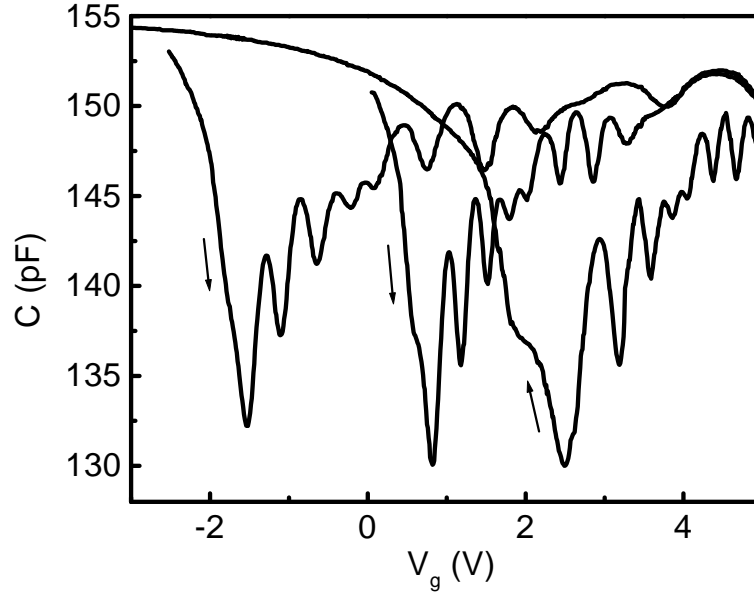


Figure 1: Capacitance-voltage dependencies in magnetic field  $B = 4.5T$  perpendicular to 2D plane for sample  $S2$  at different gate voltage sweep. The arrows indicate the sweep direction. The sweep rate is  $2\text{ V/Min}$ .

with the same insulators.

The voltage dependence of the charge density  $eN_s(V_g)$  induced in inversion layer is sublinear. This is well demonstrated by the non-equidistance of quantum oscillations of the capacitance  $C(V_g)$  (see Fig. 1). The tunneling of electrons from the 2D layer into oxide causes a saturation of  $N_s(V_g)$  dependence at  $V_g - V_{fb} \approx (10 \div 15)\text{ V}$ . As a result, the  $N_s$  range accessible for investigations is limited by the value  $(3 \div 4) \times 10^{12}\text{ cm}^{-2}$  (in HgCdTe, values of  $N_s$  up to  $10^{13}\text{ cm}^{-2}$  can be obtained). Although the hysteresis effects hamper the measurements, the discussed physical results are not affected by the instability of band bending. Such instability is caused by the transient processes but not by degradation. In order to assure the stability of band bending during the measurement of  $C(B)$  oscillations, the sample was held at given capacitance (or voltage) for 5-15 minutes. The identity of  $C(B)$  plots registered at increasing and decreasing magnetic field (i.e. at different times) was examined for each  $C(B)$  curve. When the temperature (or angle) dependencies of  $C(B)$  oscillations were measured, the long term stability was checked by the repetitive measurement of initial (for given measurement cycle)  $C(B)$  plots (see Fig. 5). Although the  $C(V_g)$  and  $dC/dV_g(V_g)$  characteristics are history dependent, they are completely repeatable, if the voltage range, rate and direction of the sweep are the same (see Fig. 6).

As can be seen in Fig. 1, the magnitudes of capacitance in the  $C(V_g)$  oscillation extrema, corresponding to the same LL's number, are the same for the curves with different  $V_{fb}$ .  $C(B)$  oscillations (and consequently subband occupancy and surface potential) measured at the same magnitude of capacitance in a zero magnetic field  $C(0)$  are also identical no matter what the voltage (the value of the latter for any given  $C(0)$  is determined by the flat-band voltage, which is a history- and time-dependent). When the dc gate voltage (or

flat-band voltage at the same  $V_g$ ) is changed, the filling of interface states is also changed but does not respond to the ac ripple, i.e., the interface states do not contribute to the capacitance. This takes place for all frequencies and temperatures and testifies that the high-frequency conditions with respect to interface states are satisfied [21, 22]. Thus there is “one-to-one correspondence” between  $C(0)$ , band bending and surface density of 2D electrons  $N_s = \sum N_i$  ( $i$  is the 2D subband number). Owing to this we can reproduce  $C(B)$  curves (characterized by the  $C(0)$  values) at all times. The subband parameters are presented below as functions of  $N_s$ . Contrary to dependencies vs.  $V_g$ , these dependencies are not affected by the hysteresis effects or any specific parameters of MOS capacitors and are common to the given HgMnTe sample. It may be noted that the hysteresis has some positive points also. We have the possibility to investigate 2D electron gas in the same surface quantum well on the same sample but with a different interface charge. Particularly, it is important for the investigation of scattering mechanisms.

Typical  $C(B)$  oscillations for both samples at almost equal  $N_s$  are presented in Fig. 2 together with their  $1/B$  Fourier transforms. As in the case of gapless HgCdTe [4], the individual spin components have not been observed in the oscillations at any  $N_s$  even for lowest LL's. On the other hand, the oscillation beats and the Fourier spectra demonstrate distinctly the presence of two frequencies connected with the SO splitting of each 2D subband. The additional structure in Fig. 2 near the Fourier lines corresponding to  $i = 0$  subband for sample *S2* results from mixed harmonics. This structure is suppressed if the range of small magnetic fields (in which the oscillations relevant to the higher subbands are dominant) is excluded from Fourier analysis. For a sample *S1*, the intensities of  $i = 1$  and  $i = 2$  lines are small, and the above features are practically indistinguishable in the scale of Fig. 2. The surface densities in the spin-split subbands  $N_i^+$  and  $N_i^-$  determined from Fourier transforms are plotted in Fig. 3 as functions of  $N_s$ . The carrier distribution among 2D subbands is different for the two samples. The concentrations  $N_s$ , corresponding to the “starts” of excited subbands, increase with increasing doping level and agree well with the theoretical calculations, in which the bulk values of  $N_A - N_D$  are used. This fact also testifies that the disruption of stoichiometry in surface layers because of probable migration of atoms is insignificant. A discrepancy with theory is detectable only in the relative differences (splitting) of occupancies  $\Delta N_i/N_i = (N_i^- - N_i^+)/(N_i^- + N_i^+)$  in the small  $N_s$  range (see Fig. 4). Similar disagreement takes place for inversion layers on HgCdTe also. The possible reasons for such behavior are discussed in Ref. [4].

The intensities of Fourier lines for the high-energy branch  $I_i^+$  and low-energy branch  $I_i^-$  are different (see Fig. 2 and Fig. 7). At low  $N_i$ , the intensities  $I_i^+$  and  $I_i^-$  are close for  $i = 0$  subband, and  $I_i^- > I_i^+$  for excited subbands. The ratio  $I_i^-/I_i^+$  as a function of  $N_s$  for  $i = 0$  is shown in Fig. 4. The scattering of the points is due mainly to the fact that  $N_i^\pm$  values and especially the ratios  $I_i^-/I_i^+$  depend strongly (and non-monotonically) on a magnetic field range used in Fourier transform (for instance, it is clear that Fourier analysis will reveal no splitting for the range between beat nodes). Nevertheless, a decrease in  $I_i^-/I_i^+$  with increasing  $N_s$  is clearly visible. It is valid for excited subbands also.

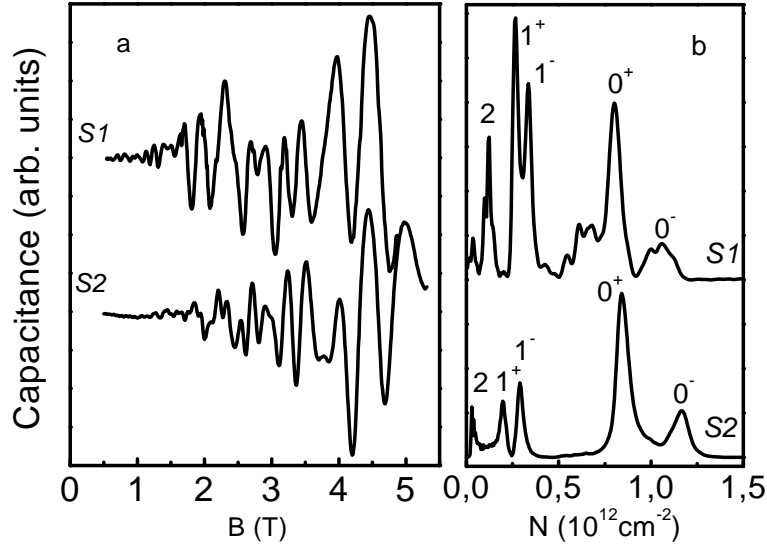


Figure 2: Capacitance oscillations (a) and their Fourier spectra (b) for  $S1$  ( $N_s = 2.76 \times 10^{12} \text{ cm}^{-2}$ ) and  $S2$  ( $N_s = 2.56 \times 10^{12} \text{ cm}^{-2}$ ) samples at close surface densities  $N_s$ . The frequency (horizontal) axis in the right panel is calibrated in the concentration units but is not normalized to the spin degeneracy. The well defined split of Fourier spectra into two lines corresponding to high-energy ( $i^+$ ) and low-energy ( $i^-$ ) branches of subband spectra is observed for subband levels  $i = 0$  and  $i = 1$ .

### 2.3 Measurements in tilted magnetic fields

Although there is no doubt that we are dealing with a 2D system (the existence of magnetooscillation effect in the capacitance and the observation of magnetooscillations versus gate voltage in itself testify to it), the fact experiments in tilted magnetic field were also performed. Some results for the sample  $S2$  are presented in Fig. 5. The magnetic field positions of the oscillation extrema and the fundament fields in the Fourier spectra (to a smaller extent) vary only roughly as cosine of the angle  $\Theta$  between  $\mathbf{B}$  and normal to the 2D layer. The clearly distinguishable deviations from such behavior are observed. Namely, the experimental angle dependencies are stronger.

There are several reasons for this deviation from classical cosine dependence, because a number of physical factors are ignored in the simplified model [23]. Firstly, in the strictest sense, such behavior, even in the case of parabolic dispersion, is valid only for an ideal 2D system. A condition to be satisfied for cosine dependence is  $\langle r \rangle / \langle z \rangle \gg 1$ , where  $\langle r \rangle$  and  $\langle z \rangle$  are the mean sizes of wave function in the 2D plane and in the confinement direction. In the case of narrow-gap semiconductors, the width of surface quantum well is relatively large and such a strong requirement may be not fulfilled (note also that  $\langle z \rangle$  is energy dependent in this case). In strong magnetic field and at small surface concentration, the cyclotron radius and the width of 2D layer may be comparably-sized (especially, for excited subbands) and diamagnetic shift must weaken the angle dependence. This is contrary to the experimental behavior. Secondly, the cosine relation is obtained for spinless particles. This is not the case in a real system. Thirdly, the SO interaction is neglected in this simple consideration. Undoubtedly, the spinlike effects can reflect on a

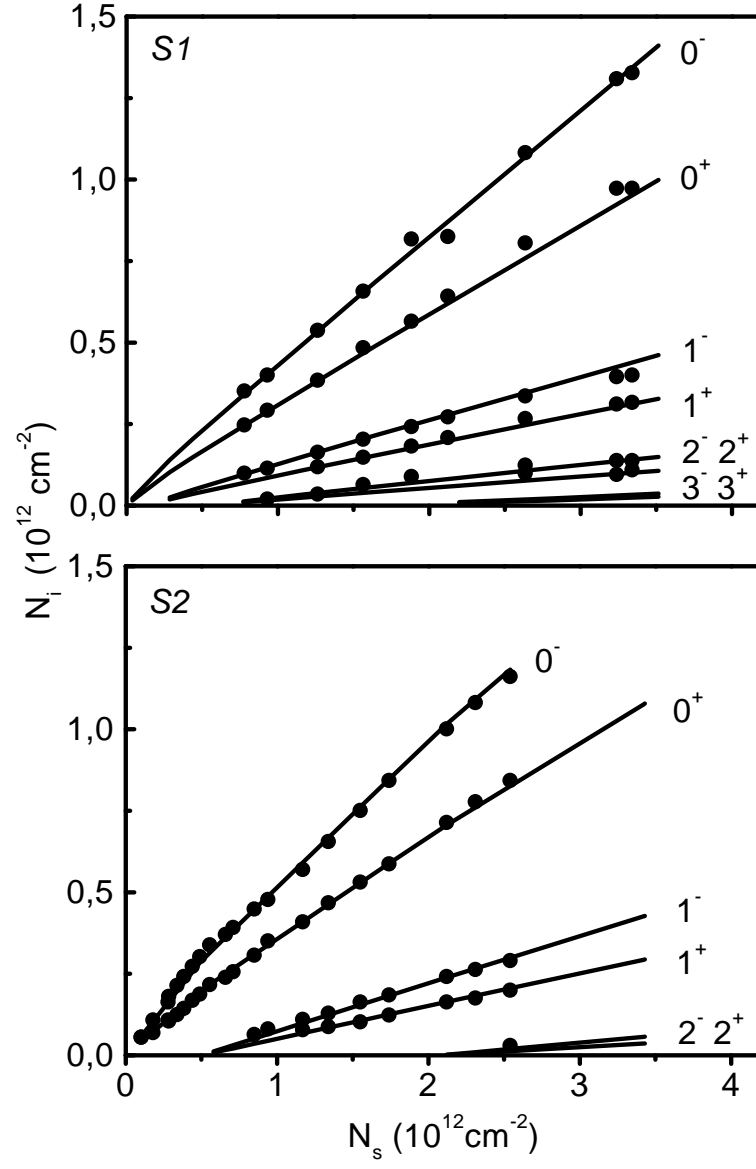


Figure 3: Calculated (lines) and measured (points) distribution of 2D electrons among the spin-split subbands  $i^\pm$  for  $S1$  and  $S2$  samples. The theoretical dependencies are calculated as in Ref. [4].



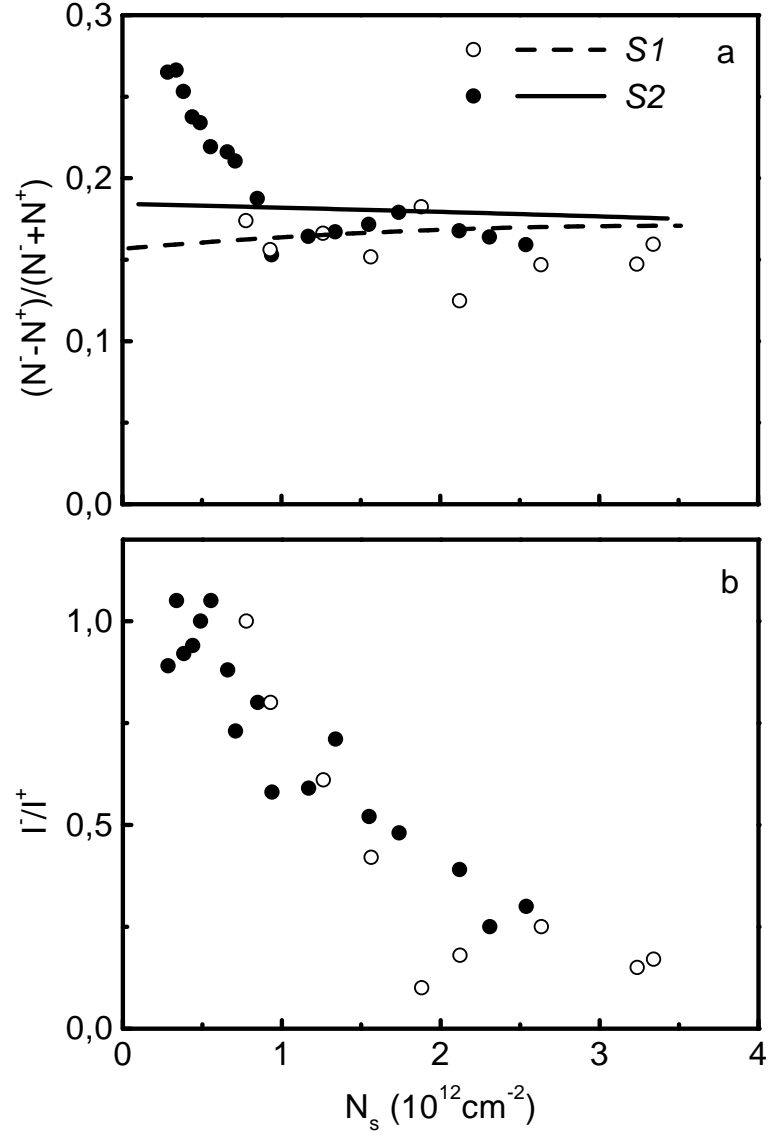


Figure 4: The relative difference of spin-split subbands occupancies (a) and the ratio of the intensities of Fourier lines for the low-energy ( $I_i^-$ ) and high-energy ( $I_i^+$ ) branches (b) versus  $N_s$  for ground subband  $i = 0$  for  $S1$  and  $S2$  samples. The lines in the upper panel are theoretical dependencies calculated as in Ref. [4].

spectrum in a tilted magnetic field and modify the angle dependence. Lastly, the exchange interaction can also make an additional contribution to the deviation from simple angle dependence. This assumption has experimental support. For comparison we investigated the HgCdTe-based samples in a tilted magnetic field. Data for HgCdTe with  $E_g = -95$  meV and  $N_A - N_D = 2 \times 10^{17} \text{ cm}^{-3}$  are given in Fig. 5. Under the same conditions they also manifest a deviation from cosine behavior. However, the deviation is weaker and opposite in sign to the case of gapless HgMnTe. At the same time, the samples based on HgCdTe with  $E_g > 0$  show a deviation of the same sign as in HgMnTe, but smaller in magnitude. Contrary to HgCdTe samples, changes in the structure of oscillations are observed in HgMnTe inversion layers. Namely, the beat nodes in oscillations  $C(B_\perp)$  ( $B_\perp = B \cos \Theta$ ) are shifted to the lower LL's numbers with increasing  $\Theta$  (i.e., with increasing total magnetic field  $B$ ) (see Fig. 5).

These experimental observations testify that the behavior in tilted magnetic fields is markedly affected by both SO interaction (which essentially depends on  $E_g$  sign, see Sec. III. and Fig. 8) and exchange interaction. For narrow-gap semiconductors, the theoretical analysis requires a consideration of spin from the outset. Strong SO and exchange interaction and resonant effects lead to serious complication of the theoretical description even for perpendicular orientation (see Sec. III.). The calculations in tilted magnetic fields are troublesome even for the simplest parabolic Hamiltonian with a  $k$ -linear Rashba term. At present we cannot make A reasonable theoretical analysis of effects in tilted fields we will restrict our consideration to the case of perpendicular orientation.

## 2.4 Temperature effects

The structure of oscillations and the subband parameters extracted from oscillations are identical to those in HgCdTe. No features due to exchange interaction are manifested. Because the exchange effects are determined by a magnetization and can be varied by the temperature, the investigation of temperature evolution of oscillations is of prime interest. The results for  $dC/dV_g(V_g)$  and  $C(B)$  oscillations are shown in Fig. 6 and Fig. 7 respectively. As it may be seen, no pronounced changes in the position of either  $dC/dV_g(V_g)$  or  $C(B)$  oscillations are observed. The shift of beat nodes to the high gate voltages and to low magnetic fields (to the greater LL's numbers) with increasing temperature (and hence with decreasing magnetization) is the sole temperature effect, besides the usual diminution of oscillation amplitudes. (Notice, the direction of shift with the increasing magnetization is similar to the one observed with increasing total  $B$  (at the same  $B_\perp$ ) in the tilted magnetic field experiments). This shift must be attributed to the features inherent in semimagnetic semiconductors because in HgCdTe-based structures neither the positions of the oscillations nor those of the beat nodes change with the temperature.

The analysis based on the Fourier transform of oscillations for different temperatures cannot yield any information about exchange interaction. On the other hand, such data cannot be obtained from spin splitting either because, as noted above, the separate spin components are not observed in the oscillations at any temperatures. Thus we must settle the question by capacitance magnetooscillations modeling.

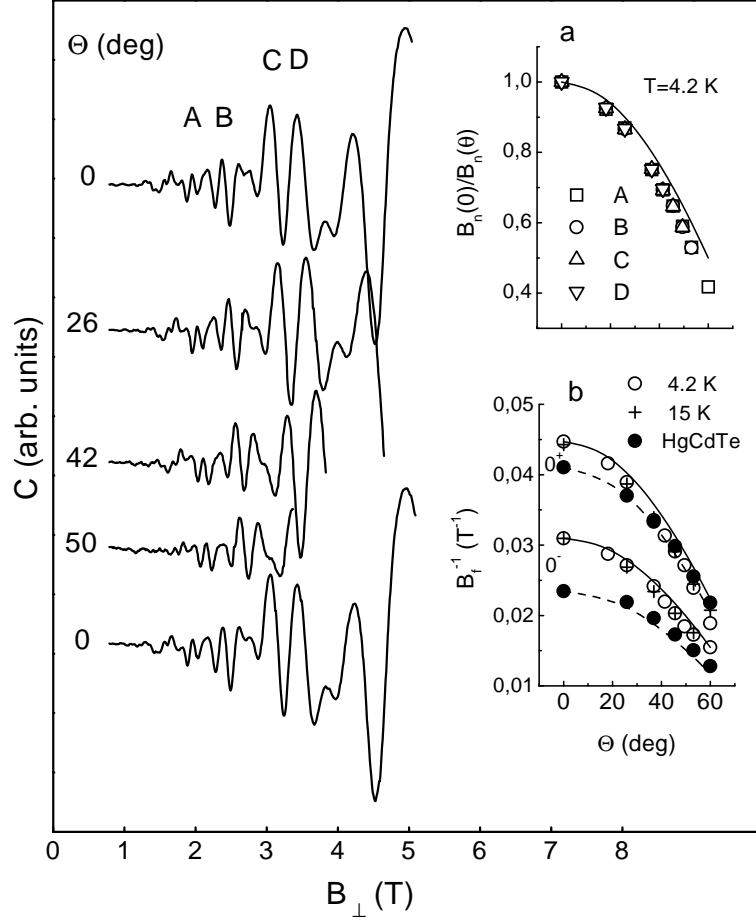


Figure 5: Capacitance oscillations plotted versus the normal component  $B_{\perp}$  of the applied magnetic field at different angles  $\Theta$  between  $\mathbf{B}$  and normal to the 2D layer for sample  $S2$  at  $N_s = 1.62 \cdot 10^{12} \text{ cm}^{-2}$ . To demonstrate the reproducibility of the results we plotted two  $C(B_{\perp})$  oscillations for  $\Theta = 0$ . The upper and lower plots are measured before and after angle dependence measurements respectively. The upper inset shows the angle dependencies  $B_n(0)/B_n(\Theta)$  for oscillation maxima marked on the upper  $C(B)$  plot. In the lower inset we plotted angle dependencies of fundamental fields in Fourier transforms for low-energy ( $0^-$ ) and high-energy ( $0^+$ ) branches of a spectrum for subband  $i = 0$ . The data for inversions layer on gapless HgCdTe at  $T = 4.2$  K are also presented (solid circles and dashed lines). The lines in the insets are cosine function.

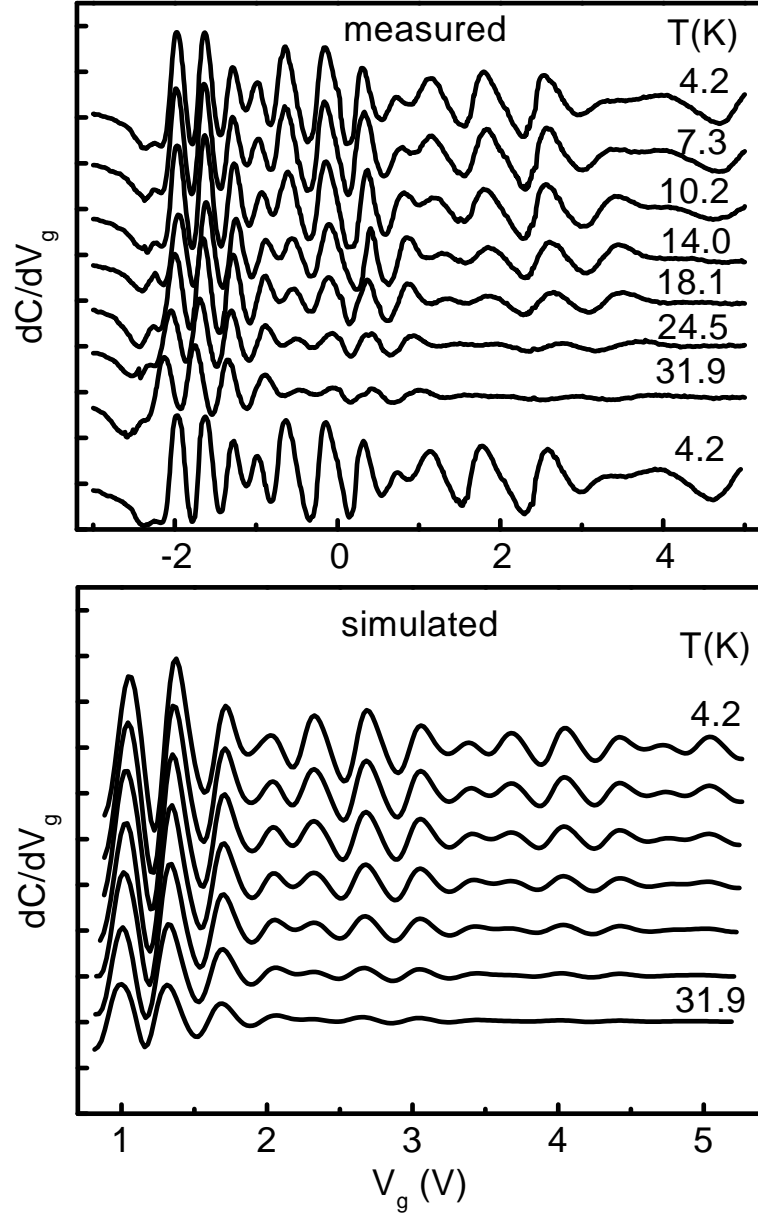


Figure 6: Experimental and simulated temperature evolution of  $\frac{dC}{dV_g}(V_g)$  oscillations in magnetic field  $B = 4$  T for sample  $S2$ . Scale division on  $\frac{dC}{dV_g}$  axis is 50 pF/V. The values  $T_N = 10$  K and  $T_D = 13$  K are used in a calculation (we neglected the weak concentration dependence of the Dingle temperature). The lower curve in the upper panel is measured two weeks later.

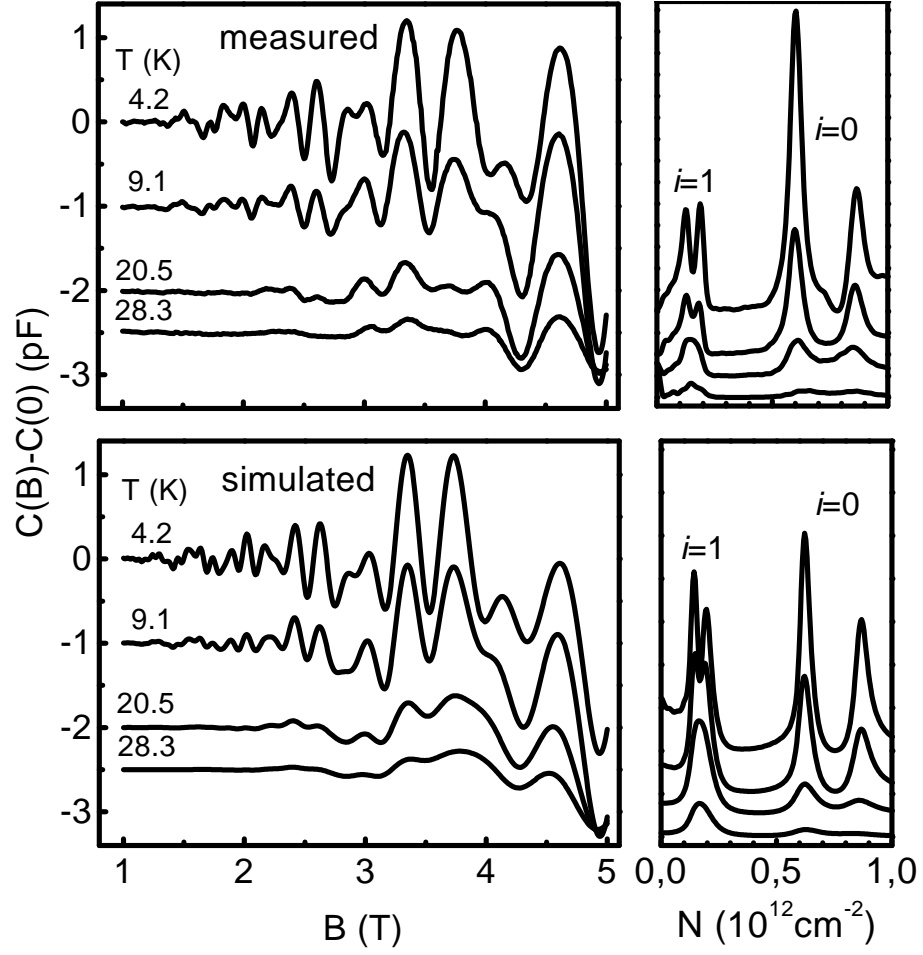


Figure 7: Experimental and simulated temperature evolution of  $C(B)$  oscillations and their Fourier spectra for sample  $S2$ . The values  $T_D = 12$  K for  $i = 0$  and  $T_D = 9.5$  K for  $i = 1$  and  $T_N = 10$  K are used in the calculation. The  $C(B)$  traces are shifted arbitrarily on  $C$  axis.

### 3 Theoretical Consideration

#### 3.1 Landau levels structure

The direct numerical solution of an initial matrix equation (especially in the case of non-zero magnetic field) faces obstacles of a fundamental nature, such as singularity problems and the ambiguity of boundary conditions on the interface and in the bulk, especially in the case of gapless semiconductors [24, 25]. In this work, we employ a concept based on the reduction of the matrix equation to a Schrodinger-like equation with an effective potential [4]. At  $B = 0$ , the results are quite close to those obtained by numeric calculations [5, 24, 26, 27]. The line of attack of Ref. [4] seems to be a reasonable compromise between accuracy and the ease of the calculation for a non-zero magnetic field. This simplicity of method is of considerable advantage for the purposes of oscillations modeling.

Under homogeneous magnetic field  $\mathbf{B}(0, 0, B)$  parallel to the direction of the confinement (surface potential  $V = V(z)$ ) a motion in the 2D plane can be quantized, using the mean field approximation for exchange interaction. It can be shown that in the framework of a six-band Kane model with an allowance for a magnetic field and exchange interaction, the following matrix equation determines the subband LL's energy  $E_n(B)$  (we do not write out the usual expressions, describing the behavior of envelopes in perpendicular to magnetic field 2D plane)

$$\begin{bmatrix} -E_- + \alpha & \frac{E_B \sqrt{3(n-1)}}{2} & \frac{E_B \sqrt{n}}{2} & 0 & 0 & s_b \hbar \hat{k}_z \\ \frac{E_B \sqrt{3(n-1)}}{2} & -E_+ + 3\beta & 0 & 0 & 0 & 0 \\ \frac{E_B \sqrt{n}}{2} & 0 & -E_+ - \beta & s_b \hbar \hat{k}_z & 0 & 0 \\ 0 & 0 & s_b \hbar \hat{k}_z & -E_- - \alpha & \frac{E_B \sqrt{3(n+1)}}{2} & -\frac{E_B \sqrt{n}}{2} \\ 0 & 0 & 0 & \frac{E_B \sqrt{3(n+1)}}{2} & -E_+ - 3\beta & 0 \\ s_b \hbar \hat{k}_z & 0 & 0 & -\frac{E_B \sqrt{n}}{2} & 0 & -E_+ + \beta \end{bmatrix} \begin{pmatrix} f_1^{n-1}(z) \\ f_3^{n-2}(z) \\ f_5^n(z) \\ f_2^n(z) \\ f_4^{n-1}(z) \\ f_6^{n-1}(z) \end{pmatrix} = 0, \quad (1)$$

where  $E_{\pm} = E_n - V \pm E_g/2$ ,  $s_b = \sqrt{|E_g|/2m_b}$  is Kane velocity,  $n$  is LL number. The envelopes  $f_{1,4}$  correspond to  $\Gamma_6$  symmetry band,  $f_{3,6}$  and  $f_{2,5}$  to heavy and light branches of  $\Gamma_8$  band. “Magnetic energy”  $E_B = \sqrt{2m_b s_b^2 \hbar \omega_b} = \sqrt{2} s_b \hbar / \lambda$  ( $\hbar \omega_b = \hbar e B / m_b c$  is cyclotron energy,  $\lambda = \sqrt{c \hbar / e B}$  is magnetic length) practically does not depend on band parameters because  $s_b$  is practically the same for all Kane semiconductors [28, 29]. We denote  $\alpha = \frac{1}{2} x N \alpha' \langle S_z \rangle$  and  $\beta = \frac{1}{6} x N \beta' \langle S_z \rangle$ , where  $x$  is the MnTe mole fraction,  $N$  is the number of unit cells per unit volume,  $\alpha'$  and  $\beta'$  are the exchange integrals for  $\Gamma_6$  and  $\Gamma_8$  bands respectively. The thermodynamically average  $\langle S_z \rangle$  of the  $z$ - component of a localized spin  $S$  (for  $\text{Mn}^{2+}$  ions  $S = \frac{5}{2}$ ) can be described via normalized Brillouin function  $B_S(x)$ :

$$\langle S_z \rangle = -S(1-x)^{18} B_S \left( \frac{2\mu_B B}{k_B(T + T_N)} \right), \quad (2)$$

where  $T_N$  is effective temperature, arising from antiferromagnetic interaction between  $\text{Mn}^{2+}$  ions [30, 31]. This factor defines the magnetic field and temperature dependency of exchange effects.

Resolving the systems (1) with respect to the components  $f_5$  and  $f_6$  we obtain the following set of two “Schrodinger-like” equations (for the envelopes  $\varphi_5^n = f_5^n/\sqrt{H_n^+}$  and  $\varphi_6^{n-1} = f_6^{n-1}/\sqrt{H_n^-}$ ) for the description of the magnetic spectrum of 2D electrons in surface layers on DMS with inverted bands (called Kane “ $p$ - electrons” as in Ref. [4])

$$\begin{vmatrix} \frac{\hbar^2 \hat{k}_z^2}{2m_b} - E_{eff} + U^+ & -iU_{so}^+ - C_g^+ s_b \hbar \hat{k}_z \\ iU_{so}^- + C_g^- s_b \hbar \hat{k}_z & \frac{\hbar^2 \hat{k}_z^2}{2m_b} - E_{eff} + U^- \end{vmatrix} \begin{pmatrix} \varphi_5^n \\ \varphi_6^{n-1} \end{pmatrix} = 0 \quad (3)$$

with effective energy

$$E_{eff} = (E^2 - m_b^2 s_b^4)/2m_b s_b^2,$$

and effective potential

$$U^\pm = U_0 + U_B^\pm + U_{exc}^\pm + U_R^\pm,$$

in which we single out the following parts: -the spin independent “Klein-Gordon“ term

$$U_0 = (V^2 - 2EV)/2m_b s_b^2,$$

and spin-like terms: “magnetic potential”

$$U_B^\pm = E_B^2 [g^2 n R^\pm + 3(n \pm 1)(E_+ \pm \beta)/(E_+ \pm 3\beta)]/2m_b s_b^2,$$

”exchange potential”

$$U_{ex}^\pm = [\alpha\beta \pm (\alpha E_+ + \beta E_-)]/2m_b s_b^2,$$

and “resonant” term describing “spin-interband“ interaction, arising from the mixing of  $\Gamma_6$  and  $\Gamma_8$  bands by an electric field

$$\begin{aligned} U_R^\pm &= \frac{s_b^2 \hbar^2}{2m_b s_b^2} \left[ \frac{3}{4} \left( \frac{1 + L_n^\pm}{H_n^\pm} \right)^2 + \frac{L_n^\pm}{H_n^\pm (E_+ \pm 3\beta)} \right] \left( \frac{dV}{dz} \right)^2 \\ &+ \frac{s_b^2 \hbar^2}{4m_b s_b^2} \frac{(1 + L_n^\pm)}{H_n^\pm} \frac{d^2 V}{dz^2}, \end{aligned}$$

where the following designations are used:

$$L_n^\pm = 3E_B^2(n \pm 1)/4(E_+ \pm 3\beta)^2, \quad H_n^\pm = E_- \pm \alpha - L_n^\pm(E_+ \pm 3\beta),$$

$$R_n^\pm = H_n^\pm/H_n^\mp, \quad g = -1$$

The spin-orbit terms and the coefficients at linear in  $\hat{k}_z$  terms are determined by

$$U_{so}^\pm = C_g s_b \hbar \sqrt{R_n^\mp} \left[ \frac{1 + L_n^\pm}{H_n^\pm} + \frac{1 + L_n^\mp}{2H_n^\mp} (R_n^\pm - 1) \right] \frac{dV}{dz},$$

$$C_g^\pm = C_g \sqrt{R_n^\mp} (R_n^\pm - 1), \quad C_g = g \frac{E_B \sqrt{n}}{4m_b s_b^2}.$$

The second term in an expression for  $U_B^\pm$  and the dimensionless parameter  $L_n^\pm$  arise from the interaction with heavy hole branch. It must be stressed that the exchange interaction causes not only the appearance of an exchange term in the effective potential, but also a modification of the terms, describing the "resonant" and SO interaction.

The LL's of 2D electrons in Kane semiconductors with  $E_g > 0$  ("s-electrons") are described by the same set (3) (for the envelopes  $\varphi_2^n = f_2^n/\sqrt{H_n^+}$  and  $\varphi_1^{n-1} = f_1^{n-1}/\sqrt{H_n^-}$ ) but with  $g = +1$ ,  $L_n^\pm = 0$ ,  $H_n^\pm = E_+ \pm \beta$ . It can be shown that the equations for Dirac like electrons in a magnetic field are the same as for Kane "s- electrons" but with  $g = +2$ . It should be emphasized that unlike the  $B = 0$  case [4], the set (3) cannot be separated and reduced to independent equations for individual spin components because of the SO interaction  $U_{so}^\pm$  (for "p- electrons", because of linear in  $\hat{k}_z$  terms also).

From this point on, we shall restrict our consideration to the semiclassical approximation just as in quantization of spectrum described by Eqs. (3) (it is clear that the use of the semiclassical approximation immediately in (1) results in the loss of spinorlike effects), so also in calculation of the surface potential  $V(z)$ . A semiclassically self-consistent potential in such treatment is calculated in the frame of quasirelativistic modification of the Thomas-Fermi method. The validity of such an approach in narrow-gap semiconductors was argued and demonstrated by a comparison with numerical self-consistent calculations in many papers [32, 33, 34] (see also Ref. [4] and references therein). Substituting as usual  $\varphi_i^m = C_i^m \exp(i \int k_z(z) dz)$  and neglecting the proportional to  $i(z dk_z/dz + k_z)^2$  terms (higher-order terms in the expansion of the action in powers of  $\hbar$ ) we obtain from (3) the quasiclassical expression for "spin-split"  $z$ -components of wave vector

$$k_z^\pm = \frac{\sqrt{2m_b s_b^2}}{s_b \hbar} \{K \mp [K^2 - (E_{eff} - U^+)(E_{eff} - U^-) + U_{so}^+ U_{so}^-]^{\frac{1}{2}}\}^{\frac{1}{2}} \quad (4)$$

with

$$K = E_{eff} - (U^+ + U^-)/2 - m_b s_b^2 C_g^2 (R_n^+ - 1)(R_n^- - 1).$$

Together with the Bohr-Sommerfeld quantization rule

$$\int_{V(z=0)}^{V(k_z=0)} k_z(E, V) \left( \frac{dV}{dz} \right)^{-1} dV = \pi \left( i + \frac{3}{4} \right) \quad (5)$$

they define the magnetic levels  $E_n^\pm(i, B)$  in surface quantum well  $V(z)$ .

For the Dirac-like electrons, the derived equations may be considered as a generalization of the result of Ref. [35] that allows for magnetic quantization and spin-like effects. In the case of Kane "s- electrons" and without exchange interaction, the Eqs. (3) and (4) coincide with the corresponding expressions in Ref. [36]. As might be expected, at  $\alpha = 0$ ,  $\beta = 0$ ,  $n \rightarrow \infty$ ,  $E_B \sqrt{n \pm 1}$  and  $E_B \sqrt{n} \rightarrow s_b \hbar k_s$  ( $k_s$  is 2D wave vector) the Eq. (5) with  $k_z$  from Eq. (4) is reduced to the corresponding equation in Ref. [4], describing subband dispersions  $E_i^\pm(k_s)$  at  $B = 0$ . Lastly, the Eq. (4) at  $V(z) = const$  determines the Landau subbands  $E_n^\pm(B, k_z)$  in the bulk of Kane (at  $\alpha = 0$  and  $\beta = 0$  non-magnetic) semiconductors.

It must be noted that the proportional to  $C_g^2$  term in expression for  $K$  (arising from linear in  $\hat{k}_z$  terms in (3)) has little effect in comparison with the spin-orbit term in Eq.



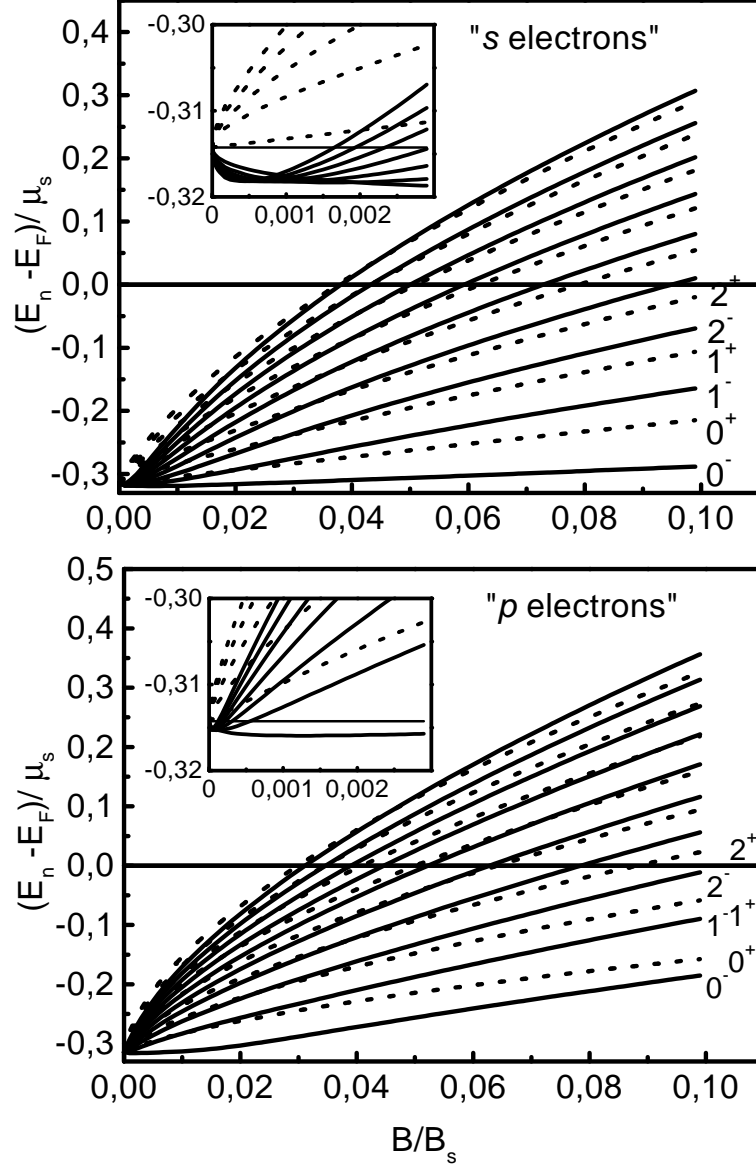


Figure 8: A spectrum in a magnetic field for Kane “*s*” and “*p* electrons” in dimensionless units in the pseudoultrarelativistic limit  $E_g = 0$ . Drastic spin-orbit perturbation of a magnetic spectrum as compared with an ordinary set of Landau levels is observed at the energies near the subband bottom [shown in insets] as well as nearby the Fermi level. The effect is essentially different for materials with direct (upper panel) and inverted (lower panel) bands.

(4). However, ignoring this term in calculations at  $U_{so}^{\pm} = 0$  can introduce large error up to the inversion of the order of spin sublevels. In pseudo-ultrarelativistic limit  $E_g = 0$  and without exchange interaction, the spectra in magnetic fields for both “s ” and “p-electrons” are scale invariant with respect to the surface band bending  $\mu_s$  as well as in the case of  $B = 0$  [4, 28]. The results for ground subband are plotted in Fig. 8 in dimensionless (normalized to  $\mu_s$ ) coordinates  $E/\mu_s - B/B_s = (E_B/\mu_s)^2$  ( $B_s = c\mu_s^2/2es_b^2\hbar$ ). It is seen that the SO interaction leads to so drastic a reconstruction of 2D spectrum in magnetic fields, that the description of spin splitting by such a non-relativistic parameter as  $g$ -factor loses in essence its physical meaning. The SO splitting far exceeds a contribution due to exchange interaction (in the scale of Fig. 8, the changes induced by exchange interaction are practically indistinguishable for reasonable exchange coupling parameters). This is true for narrow-gap DMS with  $E_g > 0$  also. In connection with this, the results of the analysis of 2D systems in asymmetrical quantum wells in these materials are to be revised, because they ignore the SO interaction.

### 3.2 Density of states and capacitance in magnetic field

For 2D systems with the multisubband spectrum, the differential capacitance of space charge region with 2D electron gas is determined by the sum  $C_{sc} = \sum C_{i\sigma}$  of “partial” subband capacitances

$$C_{i\sigma} = e^2 \frac{dN_{i\sigma}}{d\mu_s} = \frac{e^2}{\pi s^2 \hbar^2} \frac{d\mu_{Fi}}{d\mu_s} \frac{d}{d\mu_{Fi}} \int D_{i\sigma}(E) f(E - \mu_{Fi}) dE, \quad (6)$$

where  $N_{i\sigma}$  is the surface concentration in spin branch  $\sigma = \pm$  of  $i$ -th subband,  $f(E - \mu_{Fi})$  is the Fermi-Dirac distribution function and  $\mu_{Fi}$  is the subband Fermi energy. The magnetooscillations of capacitance are dictated by peculiarities in the DOS  $D_{i\sigma}(E)$  in a magnetic field, i.e. by the energy position and broadening of LL’s. The rigorous quantitative analysis of disorder broadened LL’s is a complicated problem even in one-band approximation [37, 38]. We shall perform the treatment by neglecting the mixing between LL’s and assuming a Gaussian shape of each level [39, 40]

$$D_{i\sigma} = D_i^{\pm}(E) = \frac{eB}{c\hbar\sqrt{2\pi^3}} \sum_{n=0}^{\infty} \frac{1}{\Gamma_i^{\pm}} \exp \left[ -2 \left( \frac{E - E_{ni}^{\pm}}{\Gamma_i^{\pm}} \right)^2 \right] \quad (7)$$

with broadening parameters  $\Gamma_i^{\pm}$ , independent of LL’s number, but dependent on  $B$  and (for discussed non-parabolic system) on energy. The analytical description of magnetooscillation phenomena, if possible, is preferable because it is more transparent, and easy to interpret in contrast to direct numerical methods. In addition, the peculiar features of oscillation phenomena in 2D systems with quasirelativistic spectra as compared with those of parabolic spectra [39] can thus be clarified. For this purpose we approximate the spin-split subband dispersions by analytical relativistic-like expression with the subsubband masses  $m_{0i}^{\pm}$  and velocities  $s_i^{\pm}$ . Such approximation holds for practically all the energy range of interest. The replacement in Eq.(7) of numerical solutions of Eq. (5) with  $k_z$  from Eq. (4) by the corresponding quasiclassical spectrum in a magnetic field (for simplicity we shall

drop the spin subband indices  $\sigma = \pm$  in the following)

$$E_{ni} = \sqrt{E_{Bi}^2 (n_i + \delta_i) + m_{0i}^2 s_i^4} - m_{0i} s_i^2 \quad (8)$$

( $E_{Bi} = \sqrt{2}s_i\hbar/\lambda$ ) does not noticeably reflect on the shape of the DOS. As to the LL's energy positions (and the positions of oscillations on  $B$ ), their values are to be calculated on the basis of Eqs. (4) and (5). In the Born approximation for short-range scattering, the parameter  $\Gamma_i$  is related to the classical scattering time in zero magnetic field  $\tau_i$  by  $\Gamma_i^2 = \sqrt{2/\pi}\hbar^2\omega_{ci}(E)/\tau_i$  ( $\omega_{ci}(E) = eB/cm_{ci}(E)$ ,  $m_{ci}(E) = m_{0i} + E/s_i^2$ ) [37]. Inserting the above expressions for  $E_{ni}$  and  $\Gamma_i$  in (7) and using a Poisson summation formula, we arrive (under the assumptions  $\Gamma_i \ll E_{Bi}$  and  $\Gamma_i \ll E + m_{0i}s_i^2$ , which are justified even for the states nearby the subband bottom) at a “harmonic” representation for DOS (convenient for the description of oscillation effects)

$$D_i(E, B) = D_i(E, 0)[1 + 2 \sum_{j=1}^{\infty} (-1)^j \exp\left(-\frac{j^2\pi}{\omega_{ci}(E)\tau_i}\right) \cos(2\pi j n_i(E))], \quad (9)$$

where  $D_i(E, 0) = m_{di}(E)/2\pi\hbar^2 = (E + m_{0i}s_i^2)/2\pi s_i^2\hbar^2$  is DOS at  $B = 0$ . Notice, that in the case of a two-dimension system, as is easy to show, the effective mass of DOS  $m_{di}$  coincides with the cyclotron effective mass  $m_{ci}$  for any dispersion law. The LL “number”  $n_i(E)$  in Eq. (9) is regarded as an arbitrary quantity (not necessarily an integer) and is determined at a given energy by the solutions of Eqs. (4) and (5). One can readily see that in “non-relativistic” limit ( $s_i \rightarrow \infty$ ), Eq. (9) is reduced to the Ando formula [39] if the terms with  $j > 1$  are neglected. It has been shown that for all parameters and regimes of practical interest, the DOS given by (7) and (9) are practically equivalent. This is true in the case of both the sinusoidal shape of DOS (when only ground harmonic predominates in sum (9)) and the nonsinusoidal shape of  $D(E)$  dependence. The latter case takes place at weakly broadened LL's, when the individual spin components can be resolved in total DOS.

Substituting Eq. (9) in Eq. (6) and neglecting the integrals of odd functions (this is justified at  $kT \ll \mu_{Fi}$ ) we obtain an expression for magnetocapacitance

$$\begin{aligned} \frac{C_i(B)}{C_i(0)} &= 1 - 2 \sum_j (-1)^j \exp\left(-\frac{j^2\pi}{\omega_{ci}\tau_i}\right) \int_0^\infty \frac{\cos(jb_i y)}{2 \cosh^2(y/2)} \\ &\times \{ \cos(2\pi j n_i) [\cos(2\pi j c_{Bi}^2 y^2) - (j c_{\tau i} + y c_{Ti} \tan(jb_i y)) \sin(2\pi j c_{Bi}^2 y^2)] \\ &- \sin(2\pi j n_i) [\sin(2\pi j c_{Bi}^2 y^2) + (j c_{\tau i} + y c_{Ti} \tan(jb_i y)) \cos(2\pi j c_{Bi}^2 y^2)] \} dy, \end{aligned} \quad (10)$$

where

$$\begin{aligned} y &= (E - \mu_{Fi})/kT, \omega_{ci} = \omega_{ci}(\mu_{Fi}), b_i = 2\pi kT/\hbar\omega_{ci}, \\ c_{Ti} &= K_{mi} \frac{kT}{\mu_{Fi}}, \quad c_{\tau i} = K_{mi} \frac{\hbar}{2\tau_i \mu_{Fi}}, \quad c_{Bi} = \frac{kT}{E_{Bi}} = \frac{kT\lambda}{\sqrt{2}s_i\hbar}, \\ K_{mi} &= \left[1 + \frac{d(m_{0i}s_i^2)}{d\mu_{Fi}}\right] \left[1 + \frac{m_{0i}s_i^2}{\mu_{Fi}} + \frac{d(m_{0i}s_i^2)}{d\mu_{Fi}}\right]^{-1}, \end{aligned}$$

and

$$C_i(0) = e^2 \left[ D_i(\mu_{Fi}, 0) + \frac{\mu_{Fi}}{2\pi s_i^2 \hbar^2} \frac{d(m_{0i} s_i^2)}{d\mu_{Fi}} \right] \frac{d\mu_{Fi}}{d\mu_s}.$$

Note that the identity between the capacitance in a zero magnetic field  $C_i(0)$  and the quantity  $e^2 D(\mu_F, 0) d\mu_F/d\mu_s$  breaks down in 2D systems with relativistic-like spectra [41]. As compared to the semiconductors with standard bands an expression (11) contains new parameters of the theory  $c_T$ ,  $c_\tau$  and  $c_B$ . The first and the second are due to the energy dependence of  $m_{di}$  in an expression for DOS at  $B = 0$  and of  $m_{ci}$  in exponential (Dingle) factor in Eq. (9). This energy dependence is the result of two effects. The first is the non-parabolicity of subband dispersions. The second is due to the change of the parameters of subsubband dispersions (basically  $m_{0i}^\pm(\mu_s)$ ) under the modulation of surface potential. The parameter  $c_B$  is determined in fact only by the ratio  $T/\sqrt{eB}$  and is independent of subband parameters, because  $s_i^\pm$  differs only slightly from the "universal" value of  $s_b$ . (The arising of a  $c_B$  parameter for weak relativistic Fermi gas  $\mu_F < ms^2$  of Dirac electrons is reported in Ref. [43]).

For strong enough magnetic field, the faze  $2\pi j c_B^2 y^2$  is close to zero in the range of small  $y$  (this range gives a dominant contribution to the integral in Eq. (11)) and Eq. (11) can be evaluated as

$$\frac{C_i(B)}{C_i(0)} \approx 1 - 2 \sum_j (-1)^j \frac{j\pi b_i}{\sinh(j\pi b_i)} \exp\left(-\frac{j^2\pi}{\omega_{ci}\tau_i}\right) \times [\cos(2\pi j n_i) - j c_{\tau i} \sin(2\pi j n_i)] \quad (11)$$

We point out that in the two-dimension case, the argument of the Dingle exponent is quadratic in harmonic number  $j$ . In "non-relativistic" limit  $s_i \rightarrow \infty$ , the values  $c_{Ti} = c_{\tau i} = c_{Bi} = 0$  and Eq. (11) reduces to the Ando expression for oscillations in 2D systems with parabolic spectra [37, 39]. Thus the parabolic approach is appropriate in the case of strong enough magnetic fields  $E_{Bi} > (5 \div 10)kT$  and not-too-broadened LL's ( $\hbar/2\tau_i \leq \mu_{Fi}$ ).

## 4 Results of modeling and discussion

The capacitance of the MOS structures  $C(B) = C_{ox} C_{sc}(B)/(C_{ox} + C_{sc}(B))$  was calculated using the value of oxide capacitance  $C_{ox}$ , determined from the capacitance in a strong accumulation regime. The change of charge in the depletion layer with  $\mu_s$  in the inversion band bending range (in narrow-gap semiconductors such changes can be quite significant) is taken into account in the calculation. As a rule, the theoretical capacitances  $C(0)$  are in good agreement with the ones measured at the same surface density. In a modeling, the surface potential and subband Fermi energies are supposed to be constant when a magnetic field is changing. The alternative model is based on the assumption that the surface density is fixed. However, both models give indistinguishable results at large enough LL's broadening (this is manifested by the cosine form of experimental oscillations) [42]. The temperature dependencies of band parameters and bulk Fermi energy are accounted for in the calculations.

Although the general shapes of simulated and measured oscillations  $C(B)$  are well matched, the exact magnetic field positions of the peaks and beat nodes are somewhat

different. This is not surprising, because a number of physical factors are ignored or cannot be exactly taken into account in a theory (the contribution of remote bands, interface contribution to the SO interaction (see below), the deviation of real surface potential and Landau level shape from those calculated, the superposition of oscillations from different subbands). At the same time the positions of oscillations and especially beat nodes are very sensitive to each of these factors. The adjustable phase factor (a correction  $\Delta n_i$  to LL's "number"  $n_i$  in the expressions (9), (11) and (11)) was introduced for reasons of convenience for a comparison of the temperature evolution in the measured and calculated oscillations. Its magnitude was chosen to fit the high-field node position of the beat pattern at  $T=4.2\text{ K}$ . Any physically meaningful results discussed are not affected by the choice of this factor.

The oscillations calculated with this correction and their Fourier transforms are plotted in Fig. 7. The agreement is quite good with respect to the structure of oscillations as well as the amplitudes. However, a distinguishable difference in the "number" of oscillations between beat nodes for measured and calculated plots is observed. These results, as well as the similar data on  $dC/dV_g(V_g)$  oscillations (see Fig. 6), testify to the small (but distinguishable) underestimation of SO splitting by the theory. This conclusion is valid for HgCdTe also. Note that a treatment based on the analysis of Fourier spectra does not give a clearly detectable discrepancy between experiment and theory (excluding the small  $N_s$  range (see Fig. 4)). This inconsistency with theory can be caused by the interface contribution to the SO interaction [16], which cannot be treated in the framework of effective mass method. In accordance with the experiment, the individual spin components are not exhibited in simulated  $C(B)$  or  $dC/dV_g(V_g)$  oscillations even for the lowest LL's at any reasonable broadening parameters and magnetic fields of experimental interest. The results of modeling based on Eq. (11) do not differ from the results obtained in the approximation (11) practically for all  $N_s$ ,  $T$  and  $B$  at which the oscillations are observed experimentally. As a rule, the contribution from the sine term in Eq. (11) is small.

## 4.1 Exchange interaction effects

A modeling shows that the magnetic field positions of the oscillations beyond the neighborhood of beat nodes are unaffected by the exchange effects even at the lowest temperatures. As a result these positions are temperature independent, as occurs experimentally. This is true for any available values of the exchange constants  $N\beta'$  and  $N\alpha'$  (literature data vary markedly, see Refs. [1, 44, 45] and [46] and references in these works; note that in different papers the notations for exchange constants differ in sign [1]). As noted in Sec. II, an exchange interaction is very weakly manifested in the studied system, showing itself as only a slight temperature shift of beat nodes. Because the oscillation amplitudes in the neighborhood of nodes are small even at  $T = 4.2\text{ K}$  and they decrease drastically with temperature, the narrow range of  $T < 10 \div 15\text{ K}$  is accessible to the quantitative analysis. Thus the results are not critically sensitive to a choice of  $N\beta'$  and  $N\alpha'$ . Secondly, the rate of shift depends on the product of the exchange parameters  $N\beta'$  and  $N\alpha'$  and the magnetization  $\langle S_z \rangle$ . So the variations in  $N\beta'$  and  $N\alpha'$  can be cancelled out by the variation in  $T_N$ , which is used as an adjustable parameter (see below). It must be stressed that the terms containing a parameter  $\beta$  play the dominant role in Eqs. (1), (3) and (4) for

$p$ -electrons. Under the conditions of experimental interest, the temperature shift of beat nodes is also slightly sensitive to the variations  $N\alpha'$  in a wide range even if a small  $N\beta'$  is chosen.

Although we performed the calculations for a different net of exchange parameters, the results discussed in this Section correspond to  $N\beta' = 1.5\text{ eV}$  and  $N\alpha' = -0.4\text{ eV}$ , unless otherwise specified. The results are only slightly sensitive to variances of  $N\beta'$  in the range  $1.35 \div 1.65\text{ eV}$  and do not differ at all for  $N\alpha'$  varied through  $-(0.35 \div 0.50)\text{ eV}$  range. These values are close to those obtained in Refs.[44] and [45] for narrow-gap and gapless HgMnTe with small  $|E_g|$  by the tunnel spectroscopy method. We suppose that these data (similar values for gapless HgMnTe have been obtained in many works (see Refs. [1, 44] and [45] and references in these works) are more suitable for the purposes of this work, because in studied surface quantum wells the typical electron energies are of the order of or even considerably more than  $|E_g|$ . In tunnel experiments, the LL's energy positions of “ $p$ - electrons” as a function of magnetic field are measured at energies up to 150 meV. At the same time, the states with the energy near band bottom are tested by the traditional methods.

It should be noted in connection with this that a decrease of  $|N\alpha'|$  for  $s$ -electrons in wide-gap CdMnTe-CdMgMnTe quantum well with increasing energy is reported in a recent paper Ref. [47]. The effect is attributed to the admixing of  $\Gamma_8$  band states to  $\Gamma_6$  band at finite  $\mathbf{k}$ -vectors which leads to switching-on of a kinetic exchange for electrons of  $\Gamma_6$  band with the  $d$  electrons of Mn ions. Note that in narrow-gap semiconductors, the interband mixing, described by the Kane Hamiltonian (1), results in a strong (and energy dependent) contribution of the  $N\beta'$  containing terms to a spectrum of  $\Gamma_6$  band. This is true without allowing for the energy dependence of parameter  $N\alpha'$ . As for electrons of  $\Gamma_8$  band (“ $p$ -electrons”), the value of the exchange parameter ( $N\beta'$ ) is from the outset governed mainly by kinetic exchange (at any  $\mathbf{k}$ -vector). In this case, an increase of  $\mathbf{k}$ -vector cannot play a critical role. At present, we do not have evidence of energy dependence of parameter  $N\beta'$ . The absence of an essential change in the value of  $N\beta'$  is noted in Refs. [47] and [48]. Together with the weak sensitivity of the observed effects to a choice of  $N\beta'$  and  $N\alpha'$ , this suggests that any possible energy dependence of exchange parameters cannot markedly reflect on the results.

Once the exchange parameters are chosen, two parameters can be obtained when the modeling fits experimental data: the effective temperature  $T_N$ , which describes the temperature shift of beat nodes, and the Dingle temperature  $T_D = \hbar/k_B 2\pi\tau$  (used by us as the characteristic of the scattering instead of collision time  $\tau$ ), which determines the oscillation amplitudes.

Although a decrease of magnetization with increasing temperature results in the slight energy shift of spin sublevels, the position of resulting oscillations on a magnetic field is almost unchanged (see Fig.9). The rate of shift with temperature depends on the  $N_i$  and node number, as is shown in Fig.10. At the same time, the value of  $T_N$ , extracted from the fit of the temperature evolution of oscillations, is almost the same for different nodes and  $N_i$ , which counts in favor of model used. The results of the simulation are not critically dependent on the exact value of  $T_N$  chosen. However, the “best fitting” value  $T_N = 10 \pm 1.5\text{ K}$  must be a fairly good estimation. Unfortunately, as far as we know, the low-temperature data on  $T_N$  value for bulk HgMnTe with  $x = 0.04$  are absent. Most of the

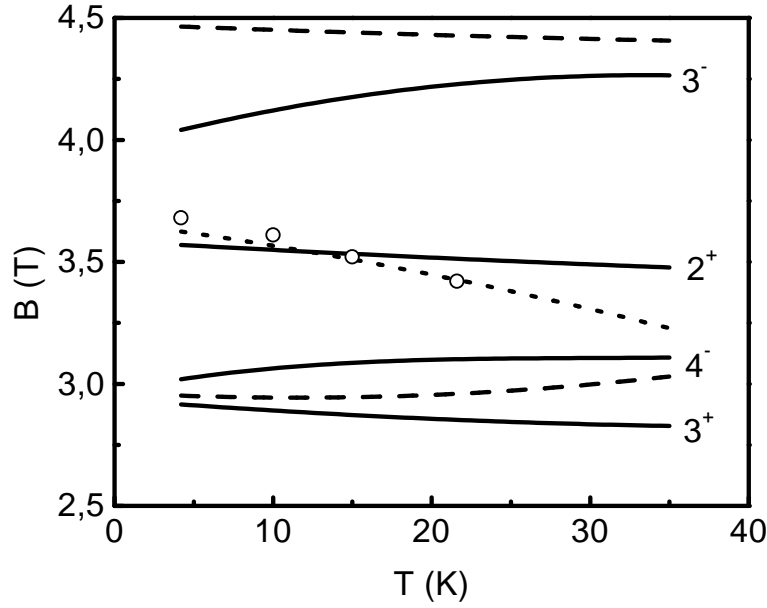


Figure 9: Magnetic field positions of the Landau levels (full curves), the maxima of simulated oscillation (broken curves) and the beat node (dotted curve) calculated as a function of the temperature for ground subband at subband occupancy  $N_0 = 0.59 \times 10^{12} \text{ cm}^{-2}$  (sample *S2*).  $T_N = 10 \text{ K}$ . The experimental positions of the beat node are shown as points.

literature data are obtained either for high temperatures or for samples with Mn content  $x \leq 0.025$ . However the value  $T_N = 10 \text{ K}$  does not contradict other published data. If the sample-independence of spin-spin interaction is postulated,  $T_N$  is nearly proportional to  $x(1-x)^{18}$  (see Ref. [30]). Using the low temperature data from Ref. [30] for a sample with  $x = 0.01$  ( $T_N = 2.9 \text{ K}$  at  $T = 2 \text{ K}$ ) we can estimate the value of  $T_N$  for samples with  $x = 0.04$  as  $T_N \approx 8 \text{ K}$ . This is somewhat less than the measured value, but  $T_N$  can also be temperature dependent. [49] For example, for the same sample with  $x = 0.01$ ,  $T_N$  is equal to  $7 \text{ K}$  in a high temperature range [30]. It must be noted that the above estimations are based on assumptions which can be violated (including a phenomenological expression itself (2)) for  $x > 0.02$  and low temperature.

The SO interaction not only contributes predominantly to the spin splitting but also suppresses the splitting due to exchange interaction. As an example, the SO splitting, corresponding to the first beat node in Fig. 7, is  $24.9 \text{ meV}$ . If we take exchange interaction into account, the splitting increases by only  $3.7 \text{ meV}$  even at  $T = 4.2 \text{ K}$ . At the same time, the exchange splitting, calculated without allowance for SO interaction, is  $6.4 \text{ meV}$ . That is why the exchange effects show themselves only as a weak change in the structure of oscillations near the beat nodes, where the oscillations from different spin branches quench each other.

Let us now return to the dependence of observed exchange effects (the temperature shift of beat nodes) on the value of exchange parameters. Only the shift of beat nodes to low LL's numbers is observed at low temperatures with decreasing  $N\beta'$  (the shift is slightly sensitive to the variations  $N\alpha'$  in  $-(0.25 \div 0.5) \text{ eV}$  range). As a result, the rate of temperature shift of nodes decreases and becomes less than the one calculated at  $N\beta' =$

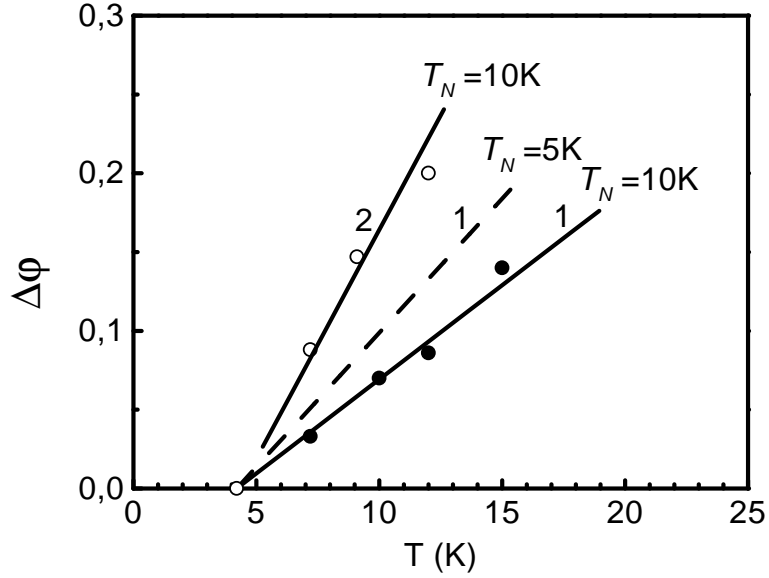


Figure 10: Calculated (curves) and measured (points) temperature shift of magnetic field position of the beat node (in the units of fundamental period) at  $N_0 = 1.45 \times 10^{12} \text{ cm}^{-2}$  (curves 1) and  $N_0 = 0.59 \times 10^{12} \text{ cm}^{-2}$  (curve 2) for sample *S2*.

1.5 eV. However, at  $N\beta' > 0.75 \text{ eV}$ , this decrease can be cancelled out by a decrease in  $T_N$ . For  $N\beta' = 1.0 \text{ eV}$  and  $N\alpha' = -0.4 \text{ eV}$  the shifts coincide with those found for  $N\beta' = 1.5 \text{ eV}$  and  $N\alpha' = -0.4 \text{ eV}$  if the value  $T_N = 4 \text{ K}$  is chosen. The oscillations in both cases are practically the same at all  $B$  (including the ranges nearby the beat nodes) and  $T$ . Although the data do not allow a clear choice between the two, the value  $T_N = 4 \text{ K}$  seems to be too small for  $x = 0.04$ .

At the same time, the experimental results cannot be described at  $N\beta' < 0.7 \text{ eV}$ . The measured rate of shift is nearly twice as large as that calculated at  $N\beta' = 0.6 \text{ eV}$  and  $N\alpha' = -0.4 \text{ eV}$  (the values given in Ref. [46]) even if  $T_N = 0$  is chosen. Although the exchange effects in studied systems with a strong interband mixing are suppressed by SO splitting, such a discrepancy is beyond the limits of experimental error. It is easy to verify that the experimental data (energy position of LL's and its temperature shift) presented in Refs. [44] and [45] for bulk HgMnTe with small  $|E_g|$  also cannot be explained at  $N\beta' < 1.0 \div 1.2 \text{ eV}$  even for  $T_N = 0$ . As already noted, the value of  $N\beta'$  reported in works on gapless HgMnTe falls typically within  $0.9 \div 1.6 \text{ eV}$ .

## 4.2 Dingle temperature and scattering

At calculations we suppose that  $T_D$  for both spin-orbit branches is the same, as it occurs for light and heavy holes in the bulk of a semiconductor. This assumption has supporting experimental evidence. When three or more beat nodes are observed in the oscillations, the “partial” oscillations relating to different spin branches can be extracted from experimental  $C(B)$  traces, using Fourier filtration and inverse Fourier transform. The  $T_D$  values determined from fitting turn out to be close for both branches within the accuracy of the analysis. At the same time, the amplitudes corresponding to these branches can differ



considerably (up to several times). Such a difference is not surprising. It is clear that both the DOS and cyclotron energy are different for two branches of a spectrum having significantly different dispersions. As a result, the “partial” capacitance oscillations for these branches differ not only by the period (which leads to the beat of oscillations) but also by the amplitudes, even if the relaxation times are equal. Although DOS at  $B = 0$  in a low-energy branch is higher, the corresponding amplitudes can be less, because the lower cyclotron energy in this branch leads to a lesser amplitude factor in Eqs. (11) and (11).

The relation between amplitudes depends on the subband occupancies (via the effective mass), magnetic field, temperature and broadening parameters. For different subbands,  $B$  and  $N_s$ , the ratio of amplitudes  $A_c^-/A_c^+$  can be below as well as above unity. However, the value of  $A_c^-/A_c^+$  decreases rapidly with increasing  $N_i$ . Such behavior correlates well with decreasing ratio of Fourier line intensities  $I_i^-/I_i^+$  experimentally observed (see Fig. 4). Thus the difference in the amplitudes for different spin components of oscillations mentioned in Refs. [11] and [14] is to be expected for 2D systems with strong SO interaction (without invoking spin-dependent scattering).

The Dingle temperature  $T_D$ , determined from the fitting, slightly increases (from  $8 \div 9$  to  $13 \div 15$  K for ground subband) with the increasing  $N_s$ . Such behavior is inherent in surface roughness scattering [37, 50]. The  $T_D(N_s)$  dependencies are essentially sublinear. This testifies that the efficiency of scattering is suppressed with the increasing of the Fermi wave vector. This is possible if the correlation length  $\Lambda$  is large enough. The best agreement between experimental and calculated values of  $T_D$  is achieved at  $\Lambda \approx (110 \div 120)$  Å and at the average interface displacement  $\Delta \approx (20 \div 25)$  Å. Note that the screening effects contribute significantly to the scattering, because in surface layers on narrow-gap semiconductors, the Fermi wavelength turns out to be of the same order of magnitude as 2D Thomas-Fermi screening length and  $z$ -size of wave function. The above values of  $\Lambda$  and  $\Delta$  are many times larger than those found for silicon [37] and substantially exceed the corresponding values in III-V semiconductors also [50]. This suggests much more disorder in the interface between ternary compounds and their oxides. Using the  $T_D$  values, the electron mobility can be estimated as  $0.8 \times 10^4$  cm<sup>2</sup>/Vs in  $i = 0$  subband and  $1.5 \times 10^4$  cm<sup>2</sup>/Vs in  $i = 1$  subband for sample *S1* at  $N_s \sim 10^{12}$  cm<sup>-2</sup> that is close to a value  $1 \times 10^4$  cm<sup>2</sup>/Vs measured for grain boundaries in *p*-HgMnTe with  $x = 0.1$  [7].

Somewhat larger values of  $T_D$  are detected at small surface densities  $N_s < 5 \times 10^{11}$  cm<sup>-2</sup>. The Coulomb scattering from the chargers in oxide cannot cause this, because the theoretical calculations give the values of relaxation times, which are larger by at least two orders of magnitude. This conclusion has direct experimental evidence. It can be seen in Fig. 1, that the charge localized in oxide differs by a factor of several times for different sweep cycles. If the Coulomb scattering were important, the amplitudes of oscillations corresponding to different cycles (different  $V_{fb}$ ) but to the same  $N_s$  (to the same LL's number at fixed magnetic field) would be different. Nevertheless, the oscillation amplitudes are practically the same. A possible cause for the increase of LL's broadening at small  $N_i$  is intersubband scattering [50].

**Acknowledgements.** This work was supported in part by the project Esprit N28890 NTCONGS EC (Euro Community) and by the Grant from the Education Committee of Russian Federation.

## References

- [1] For reviews of DMS and 2D DMS systems see e.g.: J.K. Furdina and J. Kossut, *Semiconductors and Semimetals*, ed. by R.K. Willardson and A.C. Beer, Academic, New York, Vol **25** (1988). J.K. Furdina, J.Vac. Sci. Technol. **A 4**, 2002 (1986).
- [2] J. Slinkman, A. Zhang, and R.E. Doezema, Phys. Rev. B, **39**, 1251 (1990)).
- [3] Y. Takada, K. Arai, and Y. Uemura, *Lecture Notes in Physics*, Proceedings of the Fourth International Conference on Physics of Narrow Gap Semiconductors, Linz, Austria, 1981 (Springer-Verlag, Berlin, 1982), Vol. **152**, p.101.
- [4] V.F. Radantsev, T.I. Deryabina, G.I. Kulaev, and E.L. Rumyantsev, Phys. Rev. B **53**, 15756 (1996).
- [5] A.V. Germanenko, G.M. Min'kov, V.A. Larionova, and O.E. Rut, Phys. Rev. B **54**, 1841 (1996).
- [6] G. Grabecki, T. Dietl, J. Kossut, and W. Zawadzki, Surf. Sci. **142**, 558 (1984).
- [7] G. Grabecki, T. Dietl, P. Sobkowicz, J. Kossut, and W. Zawadzki, Appl. Phys. Lett. **45**, 1214 (1984).
- [8] T. Suski, P. Wisniewski, L. Dmowski, G. Grabecki, and T. Dietl, J. Appl. Phys. **65**, 1203 (1989)
- [9] G. Grabecki, A. Wittlin, T. Dietl, P.A.A. Teunissen, S.A.J. Wiegers, and J.A.A.J. Perenboom, Semicond. Sci. Technol. **8**, S95 (1993).
- [10] P. Sobkowicz, G. Grabecki, T. Suski, and T. Dietl, Acta Phys. Pol. **A75**, 39 (1989).
- [11] V.F. Radantsev, T.I. Deryabina, L.P. Zverev, G.I. Kulaev, and S.S. Khomutova, Zh. Eksp. Teor. Fiz. **88**, 2088 (1985) [Sov. Phys. JETP **61**, 1234 (1985)]
- [12] Yu.A. Bychkov and E.I. Rashba, J. Phys. C. **17**, 6039 (1984).
- [13] V.F. Radantsev, Zh. Eksp. Teor. Fiz. **96**, 1793 (1989) [Sov. Phys. JETP **69**, 1012 (1989)].
- [14] J. Luo, H. Munekata, F.F. Fang, and P.J. Stiles, Phys. Rev. B **41**, 7685 (1990).
- [15] B. Das, S. Datta, and R. Reifenberger, Phys. Rev. B **41**, 8278 (1990).
- [16] G. Engels, J. Lange, Th. Schapers, and H. Luth, Phys. Rev. B **55**, R1958 (1997).
- [17] J. Nitta, T. Akazaki, H. Takayanagi, and T. Enoki, Phys. Rev. Lett. **78**, 1335 (1997).
- [18] J.P. Heida, B.J. van Wees, J.J. Kuipers, T.M. Klapwijk, and G. Borghs, Phys. Rev. B **57**, 11911 (1998)

- [19] L. Wissinger, U. Rössler, R. Winkler, B. Jusserand, and D. Richards, Phys. Rev. B **58**, 15375 (1998).
- [20] V.F. Radantsev, Semicond. Sci. Technol. **8**, 394 (1993).
- [21] R. Adar, I. Bloom and Y. Nemirovsky, Solid-St. Electron. **33**, 1197 (1990).
- [22] E.H. Nicollian and J.R. Brews, *MOS Physics and Technology*, Wiley, New York (1982).
- [23] F. Stern and W.E. Howard, Phys. Rev. **163**, 816 (1967).
- [24] P. Sobkowicz, Semicond. Sci. Technol. **5**, 183 (1990).
- [25] M.J. Godfrey and A.M. Malik, Phys. Rev. B **53**, 16504 (1996).
- [26] I. Nachev, Phys. Scr. **37**, 825 (1988).
- [27] A. Ziegler and U. Rossler, Europhysics Letters **8**, 543 (1989).
- [28] V.F. Radantsev, Pis'ma Zh. Eksp. Teor. Fiz. **46**, 157 (1987) [JETP Lett. **46**, 197 (1987)].
- [29] E.A. Jonson, A. MacKinnon, E.P. O'Reilly, and M. Silver, Phys. Rev. Lett. **65**, 752 (1990).
- [30] G. Bastard and C.J. Lewiner, J. Phys. C **13**, 1469 (1980).
- [31] D. Heiman, Y. Shapira, S. Foner, B. Khazai, R. Kershaw, K. Dwight, and A. Wold, Phys. Rev. B **29**, 5634 (1984).
- [32] T. Ando, J. Phys. Soc. Japan **54**, 2676 (1985).
- [33] V.F. Radantsev, Fiz. Tekh. Poluprov. **22**, 1796 (1988) [Sov. Phys. Semicond. **22**, 1136 (1988)].
- [34] J.P. Zollner, G. Paasch, G. Gobsch, and H. Ubensee, Phys. Stat. Sol.(b) **148**, 611 (1988).
- [35] G.I. Artimovich and V.I. Ritus, Zh. Eksp. Teor. Fiz. **104**, 2912 (1993) [Sov. Phys. JETP **77**, 348 (1993)].
- [36] F. Ohkawa and Y. Uemura, J. Phys. Soc. Japan **37**, 1325 (1974).
- [37] T. Ando, A.B. Fowler, and F. Stern, Rev. Mod. Phys. **54**, 437 (1982).
- [38] L. Spies, W. Apel, and B. Kramer, Phys. Rev. B **55**, 4057 (1997).
- [39] T. Ando, J. Phys. Soc. Jap. **37**, 1233 (1974)
- [40] R. Gerhardts, Z. Phys. B **21**, 275 (1975)

- [41] V.F. Radantsev, T.I. Deryabina, V.V. Zav'yalov, L.P. Zverev, G.I. Kulaev, and S.S. Khomutova, Fiz. Tekh. Poluprov. **23**, 346 (1989) [Sov. Phys. Semicond. **23**, 213 (1989)].
- [42] N.J. Bassom and R.J. Nicholas, Semicond. Sci. Technol. **7**, 810 (1992).
- [43] A.C. Vshivtsev and K.G. Klimenko, Pis'ma Zh. Eksp. Teor. Fiz. **109**, 954 (1996) [JETP Lett. **64**, 338 (1996)].
- [44] L.P. Zverev, V.V. Kruzhaev, G.M. Min'kov, O.E. Rut, N.P. Gavaleshko, and V.M. Frasunyak, Zh. Eksp. Teor. Fiz. **86**, 1073 (1984) [Sov. Phys. JETP **59**, 626 (1984)].
- [45] L.P. Zverev, V.V. Kruzhaev, G.M. Min'kov, O.E. Rut, N.P. Gavaleshko, and V.M. Frasunyak, Fiz. Tverd. Tela. **26**, 2943 (1984) [Sov. Phys. Solid. Stat. **26**, 1788, 1984].
- [46] J. Furdyna, J. Appl. Phys. **64**, R29 (1988).
- [47] I.A. Merkulov, D.R. Yakovlev, A. Keller, W. Ossau, J. Geurts, A. Waag, G. Landwehr, G. Karczewski, T. Wojtowicz, and J. Kossut, Phys. Rev. Lett. **83**, 1431 (1999).
- [48] A.K. Bhattacharjee, Phys. Rev. B **58**, 15660 (1998).
- [49] W. Dobrowolski, von M. Ortenberg, and A.M. Sandauer. *Lecture Notes in Physics*, Proceedings of the Fourth International Conference on Physics of Narrow Gap Semiconductors, Linz, Austria, 1981 (Springer-Verlag, Berlin, 1982), Vol. **152**, p.302.
- [50] V.F. Radantsev, T.I. Deryabina, L.P. Zverev, G.I. Kulaev, and S.S. Khomutova, Zh. Eksp. Teor. Fiz. **91**, 1016 (1986) [Sov. Phys. JETP **64**, 598 (1986)].